Fast phosphorescence from Ir(III) complexes via di-nuclear molecular design

Journal:	*Journal of the American Chemical Society*
Manuscript ID	ja-2019-07339d.R1
Manuscript Type:	Article
Date Submitted by the Author:	15-Aug-2019
Complete List of Authors:	Shafikov, Marsel; University of Regensburg Daniels, Ruth; Northumbria University, Department of Applied Sciences Kozhevnikov, Valery; Northumbria University, Department of Applied Sciences

Fast phosphorescence from Ir(III) complexes via di-nuclear molecular design

Marsel Z. Shafikov, *,†,§ Ruth Daniels,‡ and Valery N. Kozhevnikov *,‡

† *Institut für Physikalische und Theoretische Chemie, Universität Regensburg, Universitätsstrasse 31, Regensburg, D-93053, Germany. E-mail: shafikoff@gmail.com*

§ *Ural Federal University, Mira 19, Ekaterinburg, 620002, Russia.*

‡ *Department of Applied Sciences, Northumbria University, Newcastle upon Tyne, NE1 8ST, U.K. E-mail: valery.kozhevnikov@northumbria.ac.uk*

Abstract

Complexes of Ir(III) exhibiting efficient phosphorescence are highly attractive as emitters in organic light-emitting diodes (OLED). In this contribution we present the synthesis and detailed comparative investigation of two novel Ir(III) complexes featuring mono-nuclear and di-nuclear molecular design. Quantum yield and emission decay time values for the mono-nuclear complex are Φ_{PL} = 90% and τ(300 K) = 1.16 μs, while for the di-nuclear complex these values are Φ_{PL} = 95% and τ(300 K) = 0.44 μs for degassed toluene solutions at room temperature. These data show an almost three-fold increase in the phosphorescence rate for the di-nuclear complex when compared with the mono-nuclear one, indicating a stronger Spin-Orbit Coupling (SOC) of the T_1 state with singlet states. Indeed, the T_1 state Zero-Feld Splitting, that is largely the result of the SOC effect, also increases from ZFS=65 cm^{-1} for the mono-nuclear complex to a value of ZFS=205 cm^{-1} for the di-nuclear complex, accompanied by a drastic shortening of the individual decay times of T_1 sub-states. With the help of TD-DFT calculations, we rationalize that the drastic increase of $T_1 \rightarrow S_0$ radiative rate in the di-nuclear complex is a result of the much more efficient SOC of the T_1 state with excited singlet states, brought about by electronic coupling of Ir–Cl orbitals of the two coordination sites.

Introduction

Constructing molecules with the focus on emissive properties is strongly stimulated by OLED technology that demands efficient emitters for displays and artificial lighting.[1-3] During the operation of an OLED, electrically driven charge carriers (holes and electrons) have uncorrelated spins and form excitons of singlet as well as triplet multiplicity in a statistical ratio 1/3.[4] An efficient emitter must be able to utilize both types of excitons, converting their energy into light. This requirement is met in the phosphorescent complexes of transition metals, such as Ir(III) and Pt(II).[5-7] Due to strong spin-orbit coupling (SOC) induced by a heavy transition metal, these

emitters can convert singlet excitons to triplet excitons and relax from the lowest triplet state (T_1) to the ground state (S_0) via a radiative $T_1 \rightarrow S_0$ transition.[6,8,9] Indeed, cyclometallated Pt(II) and Ir(III) complexes are often employed as emitters in phosphorescent OLEDs (PhOLEDs).[7,10-28]

Apart from a high emission quantum yield, it is desirable that an OLED emitter shows a high radiative rate (short radiative decay time) in order to utilize more excitons per unit of time. For example, the well-known Ir(III) OLED emitter *fac*-Ir(ppy)$_3$ (ppy=2-phenylpyridine)[29-32] shows an emission decay time of τ = 1.6 μs and a quantum yield of Φ_{PL} = 0.9 (90%)[33,34], amounting to a radiative decay time of $\tau^r = \tau/\Phi_{PL}$ = 1.8 μs. Meanwhile, it is shown that OLED emitters with improved radiative rates are advantageous for faster utilization of excitons and suppression of triplet-triplet annihilation in the OLED's emitting layer, thus allowing the fabrication of devices operating at notably higher brightness without a loss in power efficiency.[35]

The rate of phosphorescence ($T_1 \rightarrow S_0$) is largely defined by the strength of SOC of the T_1 state with singlet states.[36] Therefore, it is an appealing idea to strengthen the SOC by molecular design. We have previously reported the modulation of T_1 state properties through ligand design in Pt(II) and Ir(III) complexes and in this paper we focus on the role of the metal and, in particular, on the effect of multinuclearity.[37,38] For the first time we experimentally demonstrate that the di-nuclear molecular design of an Ir(III) emitter can afford a fundamental advantage for faster phosphorescence in comparison to its mono-nuclear counterpart.

Results and Discussion

Chemical design and synthesis

In order to identify the significance of di-nuclear molecular design for photophysical properties, we need to use a corresponding mono-nuclear compound as a reference. For this reason, we prepared complex **5**, in which only one coordination site is engaged in coordination. The design of both complexes is largely informed by previous studies. The bridging ligand 4,6-di-(4-tert-butylphenyl)pyrimidine (dpp) has been successfully employed in the synthesis of luminescent polynuclear complexes,[39] while Haga *et. al.* previously reported bis(N-phenylbenzimidazolyl)-benzene (Phbib) as a terdentate auxiliary ligand of N^C^N coordination type.[40,41] We decided to combine these attractive structural elements and prepare mono- and di-nuclear Ir(III) complexes, **5** and **6**, for a thorough comparative study. The only minor variation is that in order to improve the solubility of the Phbib ligand, we introduced a *tert*-butyl group in the cyclometallating benzene ring. However, for the sake of clarity we will still refer to our N^C^N auxiliary ligand, 1,3-bis(N-phenylbenzimidazolyl)-5-*tert*-butylbenzene, as Phbib later in the text. Proligand **3** was prepared via the reaction of 5-*tert*-butyl isophthalic acid chloride with N-phenyl-o-phenylenediamine, followed by high temperature condensation of the intermediate in a melt at 290°C. The harsh condensation conditions are probably the reason for the low yield (25%) of the reaction. [42-45] The

reaction of the proligand **3** with iridium chloride hydrate under Nonoyama conditions (ethoxyethanol/ water, 3/1, reflux) gave the dichloro-bridged intermediate **4** in high yield. The key intermediate **4** was then reacted with two equivalents (or one equivalent for the Ir atom) of the bridging proligand 4,6-di-(4-tert-butylphenyl)pyrimidine, in presence of silver triflate as chloride scavenger, to give the mono-nuclear complex **5**, which was purified by column chromatography. The use of one equivalent of the bridging proligand **3** lead to the di-nuclear complex **6** in high yield. Both complexes are fully characterised by ^{1}H NMR spectroscopy, mass-spectrometry, elemental analysis and single crystal X-ray diffraction (XRD) analysis.

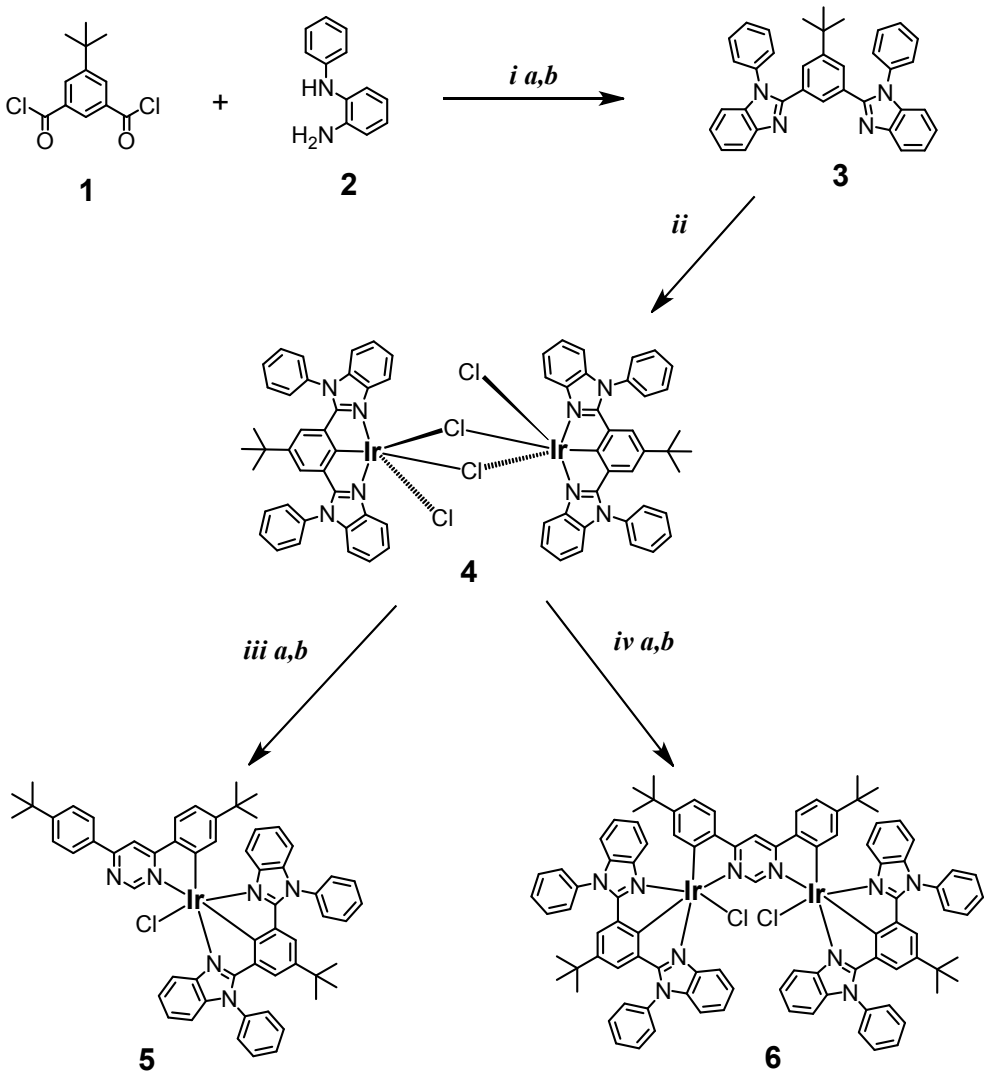

Scheme 1: Synthesis of complexes **5** and **6**. Reaction conditions: i) a)1-methyl-2-pyrrolidinone, RT, 2h; b) 290°C, 2h, 29% overall; ii) $IrCl_3 \cdot nH_2O$, ethoxyethanol/water (3/1 v/v), reflux, 18h, 89%; iii) a) 4,6-di-(4-tert-butylphenyl)pyrimidine (2 eq.,), silver triflate (3 eq.), toluene, reflux 18 h; b) HCl, 25% overall; iv) a) 4,6-di-(4-tert-butylphenyl)pyrimidine (1 eq.,), silver triflate (3 eq.), xylene, reflux 8 h; b) HCl, 91% overall.

Solid state structure

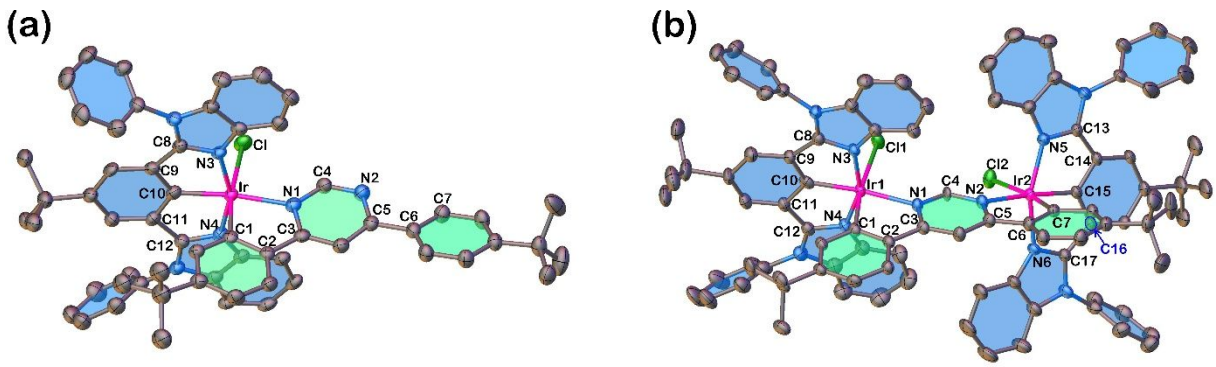

Figure 1. XRD determined molecular structure of complex **5** (a) and complex **6** (b) in the crystal at T = 123 K. Thermal ellipsoids are shown at the 50% probability level, and hydrogen atoms are omitted for clarity.

The X-ray quality crystals of **5** and **6** were both obtained in the same way, by slow convectional diffusion of methanol into a dichloromethane solution of the complex. The detailed description of the X-ray diffraction analyses and the data obtained are given in the Supporting information (SI, Table S1). The crystal of complex **5** has an asymmetric unit cell containing two independent molecules. However, the geometrical parameters of the two molecules are nearly identical (Table S2 in the SI), and further we will refer only to one of them (Molecule 1 in Table S2). The coordination centre of **5** has octahedral geometry, as expected for an Ir(III) complex. Due to the strong trans influence of the central metallating rings of ligands, the metallated carbon atoms position themselves cis- to each other. The Phbib ligand is coordinated with Ir–N3 and Ir–N4 bond lengths of 2.049 Å and 2.059 Å, respectively, and with a shorter Ir–C10 bond length of 1.945 Å. The dpp ligand features slightly longer bonds with Ir-C1 and Ir-N1 being of 2.011 Å and 2.152 Å, respectively. The chloride ion is positioned *trans* to the metallated carbon of the dpp ligand (C1), with an Ir–Cl bond length of 2.458 Å. The phenyl substituents of the diazoles of the Phbib ligand are twisted from the ligand's plane by 59-80 degrees.

Overall the geometry parameters of the two coordination centres of complex **6** are similar to those found for the coordination centre of complex **5**. The Phbib1 and Phbib2 ligands, coordinated to Ir1 and Ir2 respectively, are sterically hindered by each other, thus slightly twisting the dpp ligand and the whole molecular geometry out of C_{2v} point group symmetry. A comprehensive list of coordination centre geometry parameters is given in the SI (Tables S2 and S3).

Optical spectroscopy

Both complexes show intense $T_1 \rightarrow S_0$ phosphorescence with spectral maxima at λ_{max}=558 nm and λ_{max} = 605 nm for **5** and at λ_{max}=575 nm and λ_{max} = 618 nm for **6**, as measured in degassed toluene ($c \approx 10^{-5}$ M) at room temperature (Figure 2).

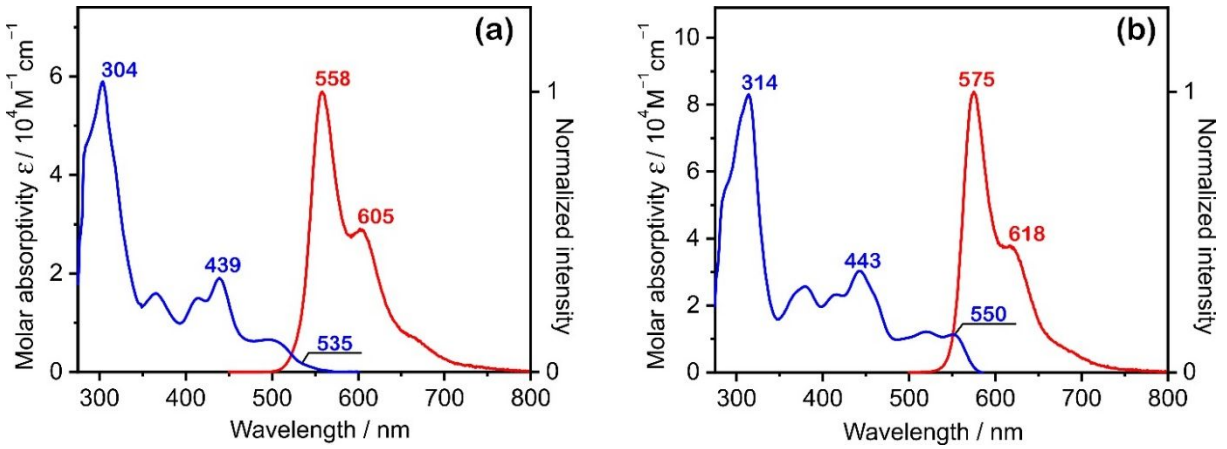

Figure 2. Absorption (blue) and emission (red) spectra of **5** (a) and **6** (b) at room temperature in toluene.

Spectral overlap of absorption and emission in both cases shows the energetic proximity of the emitting state T_1 with the manifold of excited singlet states, which is in line with the TD-DFT results. The room temperature emission quantum yields obtained for the degassed toluene solutions ($c \approx 10^{-5}$ M) amount to near unity values of $\Phi_{PL} = 0.90$ for **5** and $\Phi_{PL}=0.95$ for **6** with the corresponding emission decay times $\tau = 1.16$ µs for **5** and notably shorter value $\tau = 0.44$ µs for di-nuclear **6** (Figure 3).

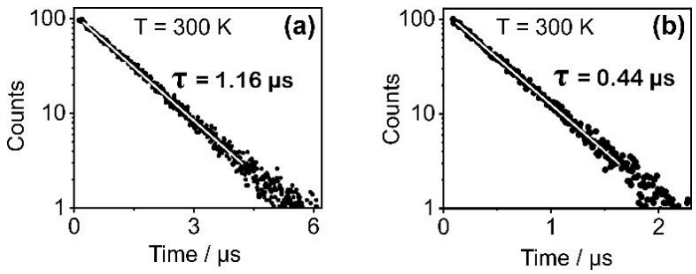

Figure 3. (a) emission decay curve of complex **5** (a) and complex **6** (b) in degassed toluene ($c \approx 10^{-5}$ M) at T=300 K. The white lines on the black experimental data points represent the best fit of mono-exponential decay function.

The resulting radiative rate $k_r = 0.78 \cdot 10^6$ s^{-1} of **5**, calculated as $k_r = \Phi_{PL}/\tau$, is a high value for phosphorescence although still comparable to other mono-nuclear Ir(III) complexes and even some polynuclear systems reported earlier[27,46]. However, the almost three times larger value $k_r = 2.27 \cdot 10^6$ s^{-1} of the di-nuclear **6** is remarkable. Along with the k_r value, the non-radiative $T_1 \rightarrow S_0$ relaxation rate, calculated as $k_{nr} = (1-\Phi_{PL})/\tau$, assuming a unit population of the T_1 state, also

increases from k_{nr} =0.86·10^5 s^{-1} for **5** to k_{nr} = 1.10·10^5 s^{-1} for **6**. The larger k_r and k_{nr} values of **6** are experimental evidence of a more relaxed ΔS=0 law for the $T_1 \rightarrow S_0$ transition. The numerical data for the photophysical properties of **5** and **6** are summarized in Table 1.

Table 1. Numerical photophysical data for photoluminescent properties of complexes **5** and **6** in toluene (c ≈ 10^{-5} M).

		5	**6**
Emission at	λ_{max} / nm	558, 605	575, 618
300 K*	τ / μs	1.16	0.44
	Φ_{PL} / %	90	95
	$k_r/10^6$ s^{-1}	0.78	2.27
	$k_{nr}/10^5$ s^{-1}	0.86	1.10
Emission at	λ_{max} / nm	543, 590, 645	565, 612
77 K	τ / μs	2.40	2.50
	Φ_{PL} / %	75	100

*These data are obtained for degassed solutions.

The ΔS=0 law forbidding the phosphorescence is relaxed by the SOC of the T_1 state with the singlet states. The more efficient the SOC, the faster the phosphorescence ($T_1 \rightarrow S_0$ transition). Therefore, according to the obtained phosphorescence rates, the T_1 state of complex **6** must undergo significantly stronger SOC with the singlet states than that of complex **5**. The basic aspects of SOC of states are considered in the theoretical part below. Experimentally the SOC of the T_1 state with other states (singlet and triplet) in the two discussed complexes can be evaluated and compared via the Zero-Field Splitting of its sub-states I, II and III, and their individual emission rates can evaluate the relative singlet admixture to each. Split in energy by SOC, the T_1 sub-states I, II, and III are not equally populated at low temperatures, affecting the overall $T_1 \rightarrow S_0$ phosphorescence rate. This can be traced by measuring the emission decay time as a function of temperature.[6,34,47-49]

Measured at a cryogenic temperature T=1.7 K complex **5** shows emission with a long decay time of τ(1.7K) = 97.6 μs, assigned to the lowest sub-state I, $I \rightarrow S_0$. It is noted that the observed slight deviation of the decay curve from the mono-exponential profile at short time range is related to Spin-Lattice Relaxation (SLR) processes[50,51], indicating a slow thermal relaxation of higher T_1 sub-states at T = 1.7 K (Figure 4(a)). This effect weakens quickly and is not observed at T = 5 K. With further increase in temperature from T = 1.7 K, the emission decay time of **5** decreases very steeply due to the thermal population of sub-state II and opening of the $II \rightarrow S_0$ relaxation channel.

This decrease becomes less steep in the temperature range of 8K ≤ T ≤ 12 K, where the decay time of sub-states I and II reaches an average value of τ(10 K) = 39 μs. A further increase in temperature is followed by further shortening of the emission decay time due to the thermal population of sub-state III and activation of the III→S_0 channel reaching the value of τ(120K) = 1.6 μs. The obtained temperature dependence of the emission decay time can be analyzed with equation (1), describing the thermal population of higher sub-states via Boltzmann type relation:[34,47,48]

$$\tau(T) = \frac{1 + \exp\frac{-\Delta E(II-I)}{k_B T} + \exp\frac{-\Delta E(III-I)}{k_B T}}{\frac{1}{\tau(I)} + \frac{1}{\tau(II)}\exp\frac{-\Delta E(II-I)}{k_B T} + \frac{1}{\tau(III)}\exp\frac{-\Delta E(III-I)}{k_B T}} \qquad (1)$$

Here τ(I), τ(II), τ(III) are the lifetimes of triplet sub-states I, II and III, respectively; ΔE(II−I) and ΔE(III−I) are the energy gaps between sub-states II and I, and sub-states III and I, respectively; T is the temperature; and k_B is the Boltzmann constant. Equation 1 was fitted to the measured decay time values in the temperature range 1.7K ≤ T ≤120 K, with parameter τ(I) fixed to the experimental value τ(I)=97.6 μs obtained at T=1.7 K. The best fit suggests the individual sub-state II and III decay times of τ(II) = 17 μs and τ(II) = 0.35 μs and energy gaps ΔE(II−I) = 5 cm^{-1} and ΔE(III−I) = 65 cm^{-1}. The average decay time, τ_{av}, of the three sub-states calculated as[52,53]

$$\tau_{av} = 3\left(\frac{1}{\tau(I)} + \frac{1}{\tau(II)} + \frac{1}{\tau(III)}\right)^{-1} \qquad (2)$$

amounts to τ_{av} = 1.0 μs. This value is close to the experimental room temperature decay time τ(300K) = 1.16 μs obtained for **5** in degassed toluene.

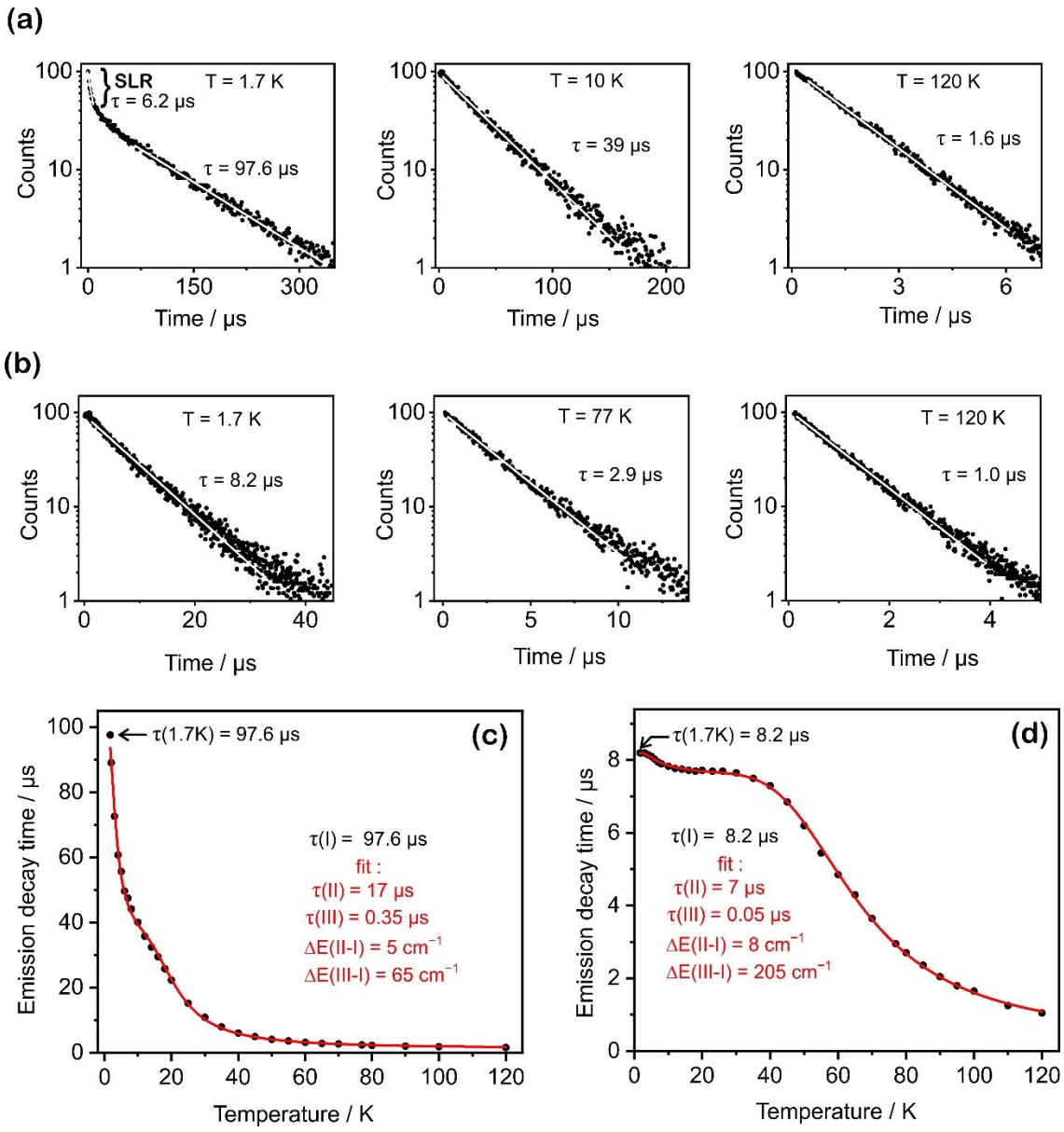

Figure 4. (a) Fitted emission decay curves of **5** in toluene at temperatures specified. **(b)** Fitted emission decay curves of **6** in toluene at temperatures specified. **(c)** Emission decay times of **5** as a function of temperature (black dots), and the best fit of Eq. 1 to the experimental values (red line). **(d)** Emission decay times of **6** as a function of temperature (black dots), and the best fit of Eq. 1 to the experimental values (red line). SLR – stands for Spin-Lattice Relaxation.

The di-nuclear complex **6** was also investigated at cryogenic temperatures. The emission decay time of **6** at T = 1.7K is τ(1.7K) = 8.2 μs. This value is constant up to a temperature of T = 3 K and is assigned to the sub-state I individual decay time, τ(I)=8.2 μs. Further increase in temperature is accompanied with a decrease of the emission decay time due to thermal activation of the II→S_0 channel. Further, in a long temperature range 12 K ≤ T ≤ 30 K, the decay times do not change strongly and form a quasi-plateau with an average I/II→S_0 decay time of τ(23K) = 7.8 μs. The

III→S_0 relaxation channel is activated at temperatures above T = 30 K and with an increase of temperature up to T = 120 K, the emission decay time decreases down to τ(120K) = 1.0 μs. The increasing population of the higher energy triplet sub-states at higher temperatures and their contribution to T_1→S_0 emission is also traced in a slight blue shift of emission spectra from T = 1.7 K to T = 77 K (Figure 5).

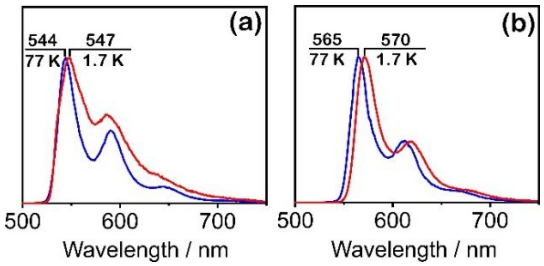

Figure 5. The emission spectra of complex **5** (a) and complex **6**(b) in toluene at 1.7 K (red trace) and at 77 K (blue trace).

The best fit of eq. 1 to the emission decay time values of complex **6** in the temperature range 1.7 K ≤ T ≤ 120 K with fixed τ(I) = 8.2 μs revealed the individual decay times τ(II) = 7.0 μs and τ(III) = 0.05 μs, and energy gaps ΔE(II−I) = 8 cm^{-1} and ΔE(III−I) = 205 cm^{-1}.

The T_1 state ZFS of 205 cm^{-1} obtained for **6** is remarkable, compared to the 65 cm^{-1} obtained for the T_1 state of complex **5**. This gives experimental evidence of a particularly strong SOC perturbation of the T_1 state. The observed increase in the ZFS value for the T_1 state of **6** has to be strongly contributed to by SOC to singlet states, as the observed individual decay times of **6** T_1 sub-states are much shorter compared to those of **5**. For example, the decay time τ(I) = 8.2 μs of **6** is an order of magnitude shorter (faster emission) than τ(I) = 97.6 μs of **5**. Moreover, the individual III→S_0 decay time of **6** as short as τ(III) = 0.05 μs shows that in this respect sub-state III behaves almost like an excited singlet state. Indeed, the theoretical analysis and computational data discussed below show that the di-nuclear structure of the complex **6** fundamentally can offer more singlet states available for direct SOC with the T_1 state, than the mono-nuclear structure of complex **5**.

The average decay time of **6** T_1 sub-states, calculated by eq. (2), amounts to τ_{av} = 0.15 μs and is 290 ns shorter than the value measured for **6** in degassed toluene at room temperature τ(300K) = 0.44 μs. For complex **5**, a deviation of τ_{av} and τ(300K) amounting to 160 ns was found. This can be rationalized by the fact that τ_{av} is calculated from data measured in the frozen media, whereas τ(300K) is measured in a liquid media condition. Solvation and molecular geometry reorganization allowed in the liquid media stabilize the excited state (T_1) and modify the T_1→S_0

transition rate. Stabilization of the T_1 state in liquid media is also seen in the red-shift of room temperature emission spectra relative to the spectra in frozen toluene matrix (compare emission spectra shown in Figure 2 and Figure 5).

Density functional calculations and theoretical considerations

To investigate the T_1 state SOC routes and to gain a profound understanding of the electronic advantage of the presented di-nuclear molecular design for enhancing the phosphorescence rate, we carried out density functional theory (DFT) calculations on both complexes, **5** and **6**. The calculations utilized Gaussian 09 code[54], Minnesota density functional M11L[55,56], def2-SVP basis set[57] and C-PCM polarizable continuum model[58] with the solvent parameters of toluene to mimic the conditions of the photophysical investigations presented above. The geometries of the complexes were optimized with "*tight*" criteria for both electronic configuration of the ground state (S_0) and the lowest triplet state (T_1) - the emitting state of phosphorescent transition metal complexes. The optimized ground state (S_0) geometries of both **5** and **6** agree well with the XRD determined geometries, with the coordination bond lengths differing by less than 0.05 Å and the coordination center angles deviating by less than 3° for three-point angles and 6° for torsion angles (Table S2 and S3 in the SI). The optimized geometries of complex **6** in S_0 and T_1 states possess a C_2 principal rotation axis, bisecting the pyrimidine ring through the C4 carbon (see Figure 1 for atom numbering) and the carbon in para-position to C4 and can be assigned to the C_2 symmetry point group. The time-dependent calculations (TD-DFT) for **5** and **6** predict the absorption spectra well, reproducing the shape of the experimental spectra. However, the lower energy bands of the theoretical spectra are slightly red-shifted, whereas the mid-range energy bands are blue shifted (See Figure S3 in the SI). Having a good agreement with the experimental data, it was assumed that the chosen theoretical method (M11L/def2-SVP/C-PCM) gives an acceptable accuracy in simulating the ground state electronic structures and excited states of both **5** and **6**.

The phosphorescence of the two complexes is best described from the perspective of the lowest triplet state (T_1), the source of $T_1 \rightarrow S_0$ phosphorescence. Accordingly, computational discussions hereafter shall refer to the optimized T_1 state geometries unless stated otherwise.

TD-DFT calculations show that the T_1 state of **5** originates from a HOMO→LUMO electronic transition, where the HOMO is an Ir–Cl anti-bonding orbital with a major Ir d-orbital contribution of 45 %, and the LUMO is a π* orbital on the Phbib ligand (Figure 6). The T_1 state of **6** is also formed of a HOMO→LUMO transition but somewhat different from that in **5.** The HOMO is an Ir1–Cl1 and Ir2–Cl2 anti-bonding orbital with total contribution from the two metals of 42% (Figure 6, Table S5). The LUMO represents a π* orbital localized, in contrast to **5**, on the dpp ligand. Thus, the T_1 state of **6** is assigned as a dπ* charge transfer character, similarly to **5**, but

with the π* this time localized on dpp ligand. It is noted that in the ground state geometry (S_0), the LUMO of **5** is also a π* orbital on dpp ligand which switches with the π* orbital on the Phbib ligand upon reorganization to the T_1 state geometry.[59] This indicates the π* orbitals of Phbib and dpp ligands in **5** are in a closer energetic proximity compared to **6**. To rationalize this difference, the π-backdonation from the metal centers to the ligands was considered. The significance of this effect can be traced by comparison of the dpp ligand structures in the two complexes. As calculated, the lowest π* orbital on the dpp ligand is antibonding to the N1–C3 and N2–C5 bonds (Figure 6 and Figures S4 and S5 in the SI) of the pyrimidine ring (See Figure 1 for atom numbering). Indeed, according to the XRD analysis, the bond lengths 1.366(4) Å for N1–C3 and 1.356(4) Å for N2–C5 in complex **5** (Molecule 1 in Table S2 in SI) increase to 1.375(4) Å for N1–C3 and to 1.374(4) Å for N2–C5 in complex **6**, where two metals coordinated to the dpp ligand. However, compared to complex **5**, the π-backdonation to the dpp ligand per metal in complex **6** is probably lower due to the steric hinderances and comparatively twisted structure of dpp. This increases the π-backdonation to the π* orbitals of Phdib1 and Phbib2 thus destabilizing those orbitals further to higher energies. Indeed, as calculated at the ground state (S_0) geometry, the lowest π* orbital on each of the Phbib ligands of **6**, representing LUMO+1 (–2.686 eV) and LUMO+2 (–2.684 eV), is destabilized compared to the lowest π* orbital on the Phbib ligand of complex **5**, representing LUMO+1 (-2.739).

Careful inspection of the higher occupied orbitals brings attention to an important difference in the electronic character and composition of complexes **5** and **6**. In the mono-nuclear complex **5**, the three t_{2g} symmetry 5d-orbitals of Ir ($5d_{xy}$, $5d_{xz}$ and $5d_{yz}$) couple pairwise with the three 3p-orbitals of the bound chloride anion and thus constitute three occupied Ir–Cl antibonding orbitals representing HOMO, HOMO–1 and HOMO–2 (Figure 6). In the di-nuclear complex **6**, however, these three occupied Ir–Cl antibonding orbitals, present at each coordination site, undergo pairwise electronic coupling that results in three pairs of molecular orbitals all involving both of the Ir ions about equally. Two molecular orbitals constituting a pair represent two possible linear combinations of two analogous Ir–Cl antibonding orbitals, and therefore involve the same Ir t_{2g} symmetry d-orbitals at the two metal centers and are different in symmetry. This is easily followed on Figure 3 where a particular Ir t_{2g} 5d-orbital contributing to HOMO–1 of complex **5**, in complex **6** contributes to HOMO–2 and HOMO–3. By the signs of orbital lobes, HOMO–2 is antisymmetric and HOMO-3 is symmetric to the C_2 rotation of **6**. The same type of symmetry is respectively valid for the HOMO and HOMO–1 pair, and for the HOMO–4 and HOMO–5 pair in complex **6** (Figure 6). The important results of the electronic coupling of the two Ir–Cl sites in complex **6** is (i) formation of three pairs of occupied molecular orbitals that approximately equally

involve both Ir ions and (ii) the two orbitals constituting a pair being contributed by Ir t_{2g} orbitals of the same angular momentum. It is shown later that this gives a larger number of excited singlet states of $^1d\pi^*$ character which are, orbital-wise, suitable for effective direct SOC with the emitting T_1 state in complex **6**.

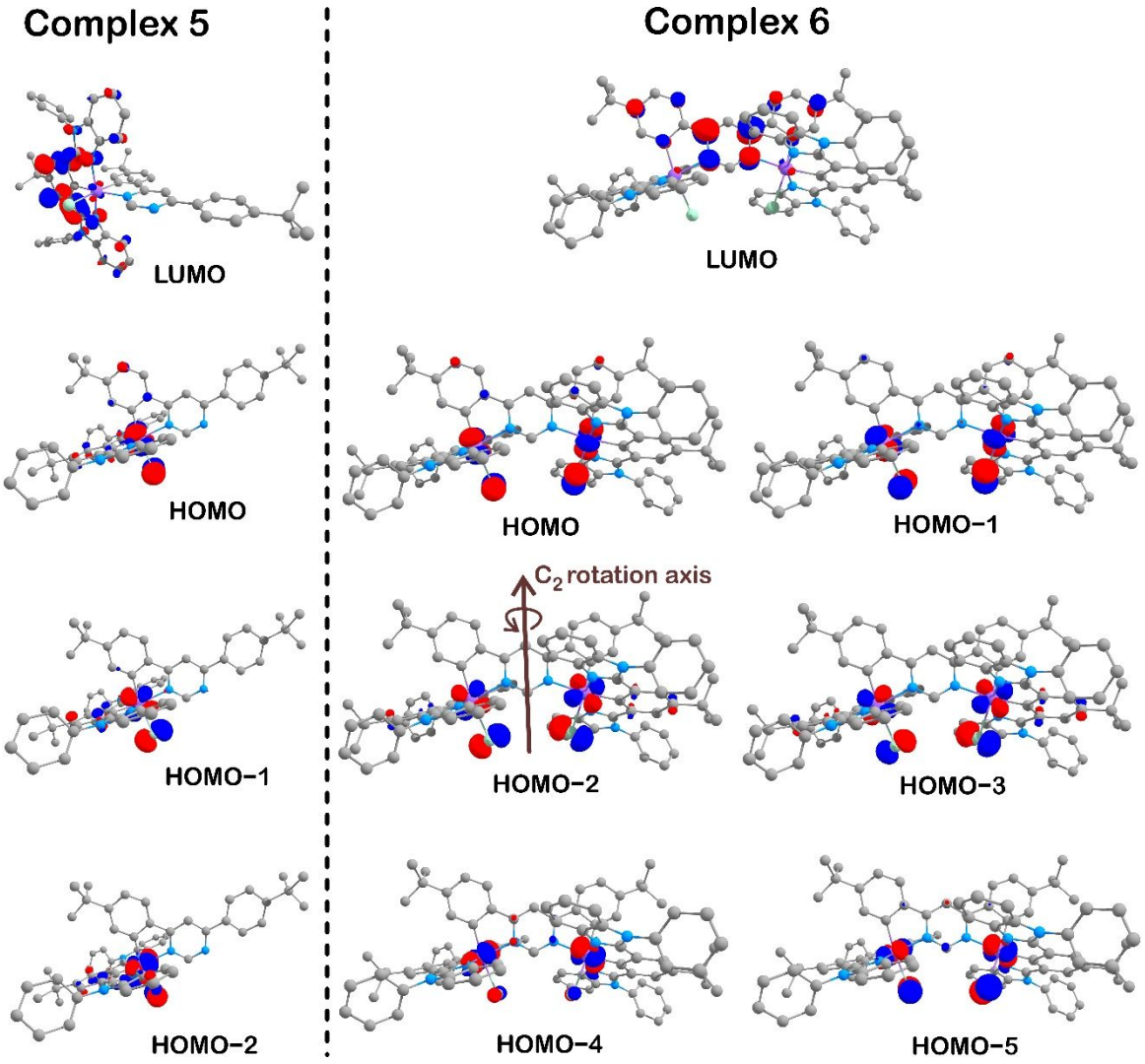

Figure 6. DFT calculated Iso-surface contour plots (iso-value=0.05) demonstrating (i) the character of the orbitals contributing to the T_1 state and singlet states that are suitable for direct SOC with the T_1 state (ii) the electronic coupling of the two Ir-Cl sites of complex **6** giving three pairs of orbitals largely contributed by t_{2g} set orbitals ($5d_{xy}$, $5d_{xz}$ and $5d_{yz}$) of the two Ir ions. Note that in **6** the same t_{2g} orbitals of the Ir ions contribute to the orbitals that constitute a pair.

The $T_1 \rightarrow S_0$ phosphorescence is a spin-forbidden process as stated by spin conservation law ($\Delta S=0$). This law, however, can be relaxed by spin-orbit coupling (SOC) of the T_1 state with states

of the singlet manifold.[36] The oscillator strength $f(T_1 \rightarrow S_0)$ (and phosphorescence rate) resulting from the SOC of the T_1 state with singlet states is defined as:[60]

$$f(T_1 \rightarrow S_0) = \sum_n \left[\left| \frac{\langle T_1 | H_{SO} | S_n \rangle}{E(S_n) - E(T_1)} \right|^2 \times f(S_n \leftrightarrow S_0) \right] \quad (3)$$

Here T_1 and $E(T_1)$ are the lowest triplet state and its energy, respectively; S_n and $E(S_n)$ are an excited singlet state and its energy, respectively; S_0 is the ground state; H_{SO} is the spin-orbit coupling operator; f is transition oscillator strength.

Considering complexes **5** and **6**, the excited singlet states in close energetic proximity to the T_1 state are of mixed dπ* and ππ* character and have non-vanishing oscillator strength $f(S_n \leftrightarrow S_0)$. Then, the SOC matrix element

$$\langle T_1 | H_{SO} | S_n \rangle$$

appears to be the main factor in formula 1 that largely defines what oscillator strength will be picked up by $T_1 \rightarrow S_0$ transition. Since SOC is a short-range interaction and H_{SO} is a one-electron operator, two states can effectively couple only if a particular heavy atom with a large SOC constant such as Ir (ζ=3909 cm^{-1})[61] contributes to the same natural transition orbital (either to hole or to electron) of both states. Then, for complexes **5** and **6**, both with a T_1 state largely of dπ* character, an effective SOC matrix element of formula 3 can be expressed as follows:

$$\langle T_1 | H_{SO} | S_n \rangle = \sum_{i,j} a_{T_1} a_{S_n} c_i c_j \langle {}^3 d_i \pi^* | H_{SO} | {}^1 d_j \pi^{*\prime} \rangle \quad (4)$$

Here a_{T_1} and a_{S_n} are normalized configurational interaction coefficients of electronic transitions contributing to the state T_1 and an excited singlet state S_n, respectively; c_i and c_j are contributions of Ir d-orbitals d_i and d_j, respectively, to the molecular orbitals involved in the transitions; π^* and $\pi^{*\prime}$ are ligand localized π-orbitals. The matrix element

$$\langle {}^3 d_i \pi^* | H_{SO} | {}^1 d_j \pi^{*\prime} \rangle$$

in formula 4 is significant only for the El-Sayed allowed cases of direct SOC with $\pi^* = \pi^{*\prime}$ and $d_i \neq d_j$ e.g. different orbital angular momentum as orbital rotation is required to conserve the total momentum of the electron (spin + orbital) when its spin flips.[6] Thus, the T_1 state can have direct SOC with a singlet state that involves a transition (i) from an Ir contributed molecular orbital different from HOMO (for $d_i \neq d_j$) to LUMO (for $\pi^* = \pi^{*\prime}$) in the case of complex **5** and, (ii) from an Ir contributed molecular orbital different from HOMO and HOMO–1 to LUMO in the case of complex **6**, as in the latter HOMO and HOMO–1 involve the Ir t_{2g} orbitals of the same angular momentum at both metal centers. TD-DFT calculations for complex **5** show one such singlet state available for direct SOC with the T_1 state: S_3 (HOMO–1→LUMO) which is within 0.5 eV energetic proximity to the T_1 state, whereas for complex **6** there are two such singlet states:

S_3 (HOMO–2→LUMO) and S_4 (HOMO–3→LUMO), which are within only 0.2 eV energetic proximity to the T_1 state (Tables S4-S7 in the SI). It is noted that the minor contribution of the HOMO–2→LUMO transition (3%) to the S_2 state of **6**, is insignificant with respect to SOC with the T_1 state, as compared to states S_3 and S_4.

The presence of two singlet states (S_3 and S_4) available for effective direct SOC with the T_1 state in complex **6** is an advantage of the presented di-nuclear design. The HOMO–2 representing the hole NTO of the S_3 state and HOMO–3 representing the hole NTO of the S_4 state are a pair of orbitals formed by electronic coupling of the two Ir–Cl sites and by the involved Ir t_{2g} orbitals, both are analogous to the HOMO–1 of complex **5** (Figure 6). In complex **5** the HOMO–1 represents the hole NTO of the S_3 state – the only singlet state available for direct SOC with the T_1 state. Thus, formation of pairs of orbitals involving the same Ir t_{2g} orbitals in the course of electronic coupling of two Ir–Cl sites in complex **6** also multiplies the number of singlet states (states S_3 and S_4 in **6** instead of only S_3 in **5**) available for direct SOC with the emitting T_1 state. Accordingly, the phosphorescence rate of **6** is notably higher than that of **5** as found experimentally. This is the fundamental advantage of the presented di-nuclear design for faster phosphorescence that opens a new avenue for the design of phosphors with enhanced efficiency. To finalize the discussion, Figure 7 gives diagrams that summarize the key results obtained in this work that provides photophysical characterization of the T_1 states of complexes **5** and **6**.

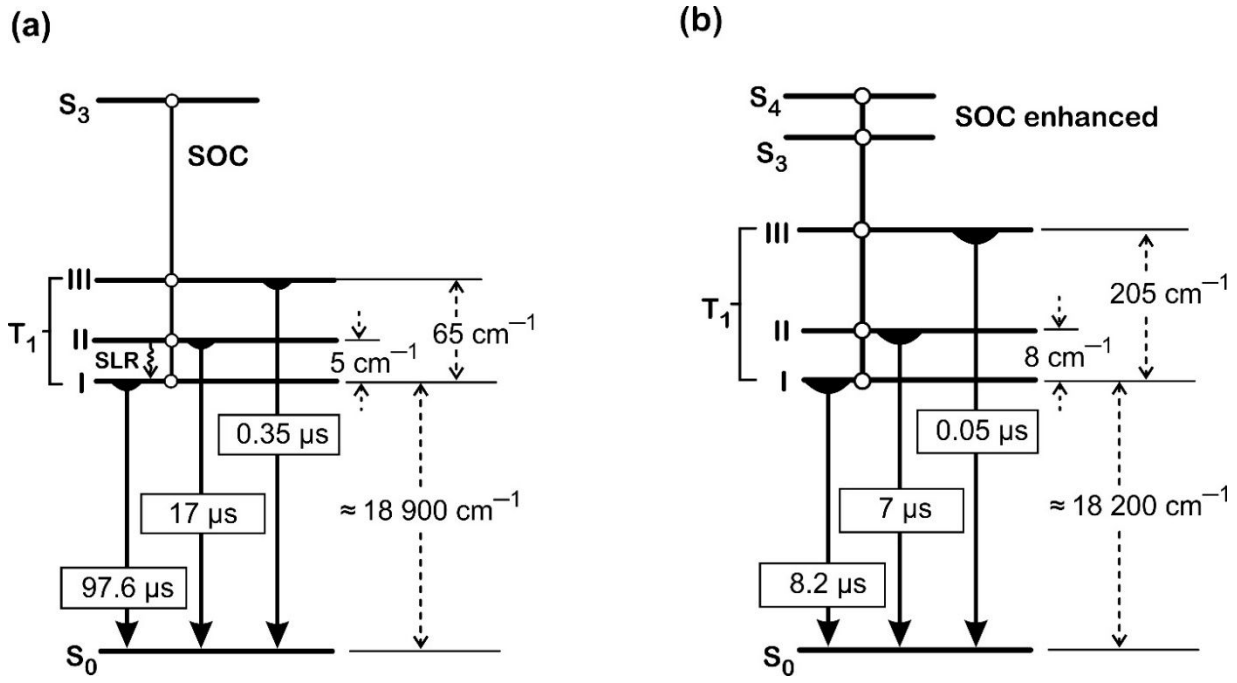

Figure 7. Simplified energy level diagrams summarizing the emissive properties of complexes **5** (a) and **6** (b) in the frozen toluene media. The diagrams are not to scale.

Concluding remarks and outlook

The Ir(III) based di-nuclear molecular design presented in this work features an electronic structure level advantage that significantly increases the phosphorescence rate. The obtained di-nuclear Ir(III) complex **6** shows a phosphorescence decay time of only 0.44 μs at 95% quantum yield. This is almost three times higher rate than of the mono-nuclear analogue with a decay time of 1.16 μs and 90% quantum yield. As suggested by TD-DFT calculations, such an improvement in the phosphorescence rate of the di-nuclear structure is due to the electronic coupling of Ir–Cl antibonding orbitals at the two coordination sites that results in three pairs of occupied molecular orbitals that are contributed to by both metal centres with the same t_{2g} orbitals in a pair. This multiplies the number of excited singlet states available for direct SOC with the emitting T_1 state, a fundamental advantage of the presented di-nuclear design for enhancing the phosphorescence rate. These computational results are in line with the experimental findings that show remarkable shortening of the individual decay times of the T_1 sub-states accompanied by a T_1 state ZFS increase from mono-nuclear **5** to di-nuclear **6**. As a result, complex **6** is an emitter with an emission rate a few times higher than other Ir(III) phosphors used in OLEDs.[10,14,17,19,21,23,25-27,29-32] Moreover, by the emission rate, **6** also outcompetes the materials exhibiting thermally activated delayed fluorescence (TADF)[62-68] which are posed as alternative OLED emitters.[62,69-72]

The proposed di-nuclear design affords outstanding phosphorescence efficiency and also leaves room for photophysical tuning through modifications of the bridging C^N–N^C ligand and N^C^N ligand and also through modifications at the position of the halogen anion. We believe that in near future the presented approach could lead to many new Ir(III) phosphors with efficiencies comparable to that of complex **6**.

ASSOCIATED CONTENT

Supporting Information

The Supporting Information is available free of charge on the
ACS Publications website at DOI:
Experimental information; Crystallographic data, DFT geometries of **5** and **6**; TD-DFT calculated theoretical absorption spectra and further output data; ^{1}H NMR characterization, mass spectrometric and elemental analysis data for **5**, **6** and intermediates (PDF)
Crystallographic data (CIF)

Accession Codes

CCDC 1922650 and 1922651 contain the supplementary crystallographic data for this paper. The data can be obtained free of charge via www.ccdc.cam.ac.uk/data_request/cif or by e-mailing

data_request@ccdc.cam.ac.uk or by contacting The Cambridge Crystallographic Data Centre, 12 Union Road, Cambridge CB2 1EZ, U.K.; fax: +44 1223 336033.

AUTHOR INFORMATION

Corresponding Authors

*E-mail: shafikoff@gmail.com (M.Z.S.), *E-mail: valery.kozhevnikov@northumbria.ac.uk (V.N.K.).

ORCID

Marsel Z. Shafikov: 0000-0003-0495-0364

Valery N. Kozhevnikov: 0000-0001-7032-8886

Notes

The authors declare no competing financial interest.

Acknowledgements

M.Z.S. gratefully acknowledges the financial by support German Research Foundation (DFG) (Project № 389797483). M.Z.S thanks Prof. Dr. Duncan Bruce and Dr. Peter B. Karadakov (The University of York, U.K.) for the help with computational facilities; Dr. Rafał Czerwieniec and Prof. Dr. Hartmut Yersin for discussions on the subject of spin-orbit coupling and zero-field splitting; Dr. Michael Bodensteiner (University of Regensburg, Central Analytical Services) for X-ray structure determination.

References

1. Sasabe, H.; Kido, J., Development of high performance OLEDs for general lighting. *J. Mater. Chem. C* **2013,** *1* (9), 1699-1707.
2. Forrest, S. R., The road to high efficiency organic light emitting devices. *Org. Electron.* **2003,** *4* (2), 45-48.
3. Adachi, C.; Baldo, M. A.; Thompson, M. E.; Forrest, S. R., Nearly 100% internal phosphorescence efficiency in an organic light emitting device. *J. Appl. Phys.* **2001,** *90* (10), 5048-5051.
4. Yersin, H., Triplet emitters for OLED applications. Mechanisms of exciton trapping and control of emission properties. *Top. Curr. Chem.* **2004,** *241*, 1-26.
5. Yersin, H., *Highly Efficient OLEDs with Phosphorescent Materials*. Wiley-VCH: Weinheim, 2008; p 458.
6. Rausch, A. F.; Homeier, H. H. H.; Yersin, H., Organometallic Pt(II) and Ir(III) triplet emitters for OLED applications and the role of spin-orbit coupling: A study based on high-resolution optical spectroscopy. *Top. Organomet. Chem.* **2010,** *29*, 193-235.
7. Li, G.; Fleetham, T.; Li, J., Efficient and Stable White Organic Light-Emitting Diodes Employing a Single Emitter. *Adv. Mater.* **2014,** *26* (18), 2931-2936.
8. Minaev, B.; Baryshnikov, G.; Agren, H., Principles of phosphorescent organic light emitting devices. *Phys. Chem. Chem. Phys.* **2014,** *16* (5), 1719-1758.

9. Lamansky, S.; Djurovich, P.; Murphy, D.; Abdel-Razzaq, F.; Lee, H. E.; Adachi, C.; Burrows, P. E.; Forrest, S. R.; Thompson, M. E., Highly phosphorescent bis-cyclometalated iridium complexes: Synthesis, photophysical characterization, and use in organic light emitting diodes. *J. Am. Chem. Soc.* **2001,** *123* (18), 4304-4312.
10. Song, J.; Kim, K.-H.; Kim, E.; Moon, C.-K.; Kim, Y.-H.; Kim, J.-J.; Yoo, S., Lensfree OLEDs with over 50% external quantum efficiency via external scattering and horizontally oriented emitters. *Nat. Commun.* **2018,** *9* (1), 3207.
11. Fleetham, T.; Ecton, J.; Wang, Z.; Bakken, N.; Li, J., Single-Doped White Organic Light-Emitting Device with an External Quantum Efficiency Over 20%. *Adv. Mater.* **2013,** *25* (18), 2573-2576.
12. Li, G.; Fleetham, T.; Turner, E.; Hang, X. C.; Li, J., Highly efficient and stable narrow-band phosphorescent emitters for oled applications. *Adv. Opt. Mater.* **2015,** *3* (3), 390-397.
13. Kalinowski, J.; Fattori, V.; Cocchi, M.; Williams, J. A. G., Light-emitting devices based on organometallic platinum complexes as emitters. *Coord. Chem. Rev.* **2011,** *255* (21), 2401-2425.
14. Tan, G.; Chen, S.; Sun, N.; Li, Y.; Fortin, D.; Wong, W.-Y.; Kwok, H.-S.; Ma, D.; Wu, H.; Wang, L.; Harvey, P. D., Highly efficient iridium(III) phosphors with phenoxy-substituted ligands and their high-performance OLEDs. *J. Mater. Chem. C* **2013,** *1* (4), 808-821.
15. Zhang, J.; Zhu, X.; Zhong, A.; Jia, W.; Wu, F.; Li, D.; Tong, H.; Wu, C.; Tang, W.; Zhang, P.; Wang, L.; Han, D., New platinum(II) one-armed Schiff base complexes for blue and orange PHOLEDs applications. *Org. Electron.: phys. mater. appl.* **2017,** *42*, 153-162.
16. Tseng, C.-H.; Fox, M. A.; Liao, J.-L.; Ku, C.-H.; Sie, Z.-T.; Chang, C.-H.; Wang, J.-Y.; Chen, Z.-N.; Lee, G.-H.; Chi, Y., Luminescent Pt(II) complexes featuring imidazolylidene-pyridylidene and dianionic bipyrazolate: from fundamentals to OLED fabrications. *J. Mater. Chem. C* **2017,** *5* (6), 1420-1435.
17. Tang, M. C.; Chan, A. K. W.; Chan, M. Y.; Yam, V. W. W., Platinum and Gold Complexes for OLEDs. *Top. Curr. Chem.* **2016,** *374*.
18. Brandt, J. R.; Wang, X.; Yang, Y.; Campbell, A. J.; Fuchter, M. J., Circularly Polarized Phosphorescent Electroluminescence with a High Dissymmetry Factor from PHOLEDs Based on a Platinahelicene. *J. Am. Chem. Soc.* **2016,** *138* (31), 9743-9746.
19. Cui, L.-S.; Liu, Y.; Liu, X.-Y.; Jiang, Z.-Q.; Liao, L.-S., Design and Synthesis of Pyrimidine-Based Iridium(III) Complexes with Horizontal Orientation for Orange and White Phosphorescent OLEDs. *ACS Appl. Mater. Interfaces* **2015,** *7* (20), 11007-11014.
20. Nisic, F.; Colombo, A.; Dragonetti, C.; Roberto, D.; Valore, A.; Malicka, J. M.; Cocchi, M.; Freeman, G. R.; Williams, J. A. G., Platinum(II) complexes with cyclometallated 5-π-delocalized-donor-1,3-di(2-pyridyl)benzene ligands as efficient phosphors for NIR-OLEDs. *J. Mater. Chem. C* **2014,** *2* (10), 1791-1800.
21. Cherpak, V.; Stakhira, P.; Minaev, B.; Baryshnikov, G.; Stromylo, E.; Helzhynskyy, I.; Chapran, M.; Volyniuk, D.; Tomkuté-Lukšiené, D.; Malinauskas, T.; Getautis, V.; Tomkeviciene, A.; Simokaitiene, J.; Grazulevicius, J. V., Efficient "warm-white" OLEDs based on the phosphorescent bis-cyclometalated iridium(III) complex. *J. Phys. Chem. C* **2014,** *118* (21), 11271-11278.
22. Kui, S. C. F.; Chow, P. K.; Cheng, G.; Kwok, C.-C.; Kwong, C. L.; Low, K.-H.; Che, C.-M., Robust phosphorescent platinum(II) complexes with tetradentate O^N^C^N ligands: high efficiency OLEDs with excellent efficiency stability. *Chem. Commun.* **2013,** *49* (15), 1497-1499.
23. Gildea, L. F.; Williams, J. A. G., Iridium and Platunum Complexes for OLEDs. In *Organic light-emitting diodes: materials, devices and applications*, A., B., Ed. Woodhead Publishing: Cambridge, 2013; pp 77-113.
24. Mróz, W.; Botta, C.; Giovanella, U.; Rossi, E.; Colombo, A.; Dragonetti, C.; Roberto, D.; Ugo, R.; Valore, A.; Williams, J. A. G., Cyclometallated platinum(II) complexes of 1,3-di(2-pyridyl)benzenes for solution-processable WOLEDs exploiting monomer and excimer phosphorescence. *J. Mater. Chem.* **2011,** *21* (24), 8653-8661.

25. Lamansky, S.; Kwong, R. C.; Nugent, M.; Djurovich, P. I.; Thompson, M. E., Molecularly doped polymer light emitting diodes utilizing phosphorescent Pt(II) and Ir(III) dopants. *Org. Electron.* **2001,** *2* (1), 53-62.
26. Adachi, C.; Baldo, M. A.; Forrest, S. R.; Lamansky, S.; Thompson, M. E.; Kwong, R. C., High-efficiency red electrophosphorescence devices. *Appl. Phys. Lett.* **2001,** *78* (11), 1622-1624.
27. Liao, J. L.; Rajakannu, P.; Gnanasekaran, P.; Tsai, S. R.; Lin, C. H.; Liu, S. H.; Chang, C. H.; Lee, G. H.; Chou, P. T.; Chen, Z. N.; Chi, Y., Luminescent Diiridium Complexes with Bridging Pyrazolates: Characterization and Fabrication of OLEDs Using Vacuum Thermal Deposition. *Adv. Opt. Mater.* **2018,** *6* (11), 1800083.
28. Tuong Ly, K.; Chen-Cheng, R.-W.; Lin, H.-W.; Shiau, Y.-J.; Liu, S.-H.; Chou, P.-T.; Tsao, C.-S.; Huang, Y.-C.; Chi, Y., Near-infrared organic light-emitting diodes with very high external quantum efficiency and radiance. *Nat. Photon.* **2016,** *11* (1), 63-69.
29. Baldo, M. A.; Lamansky, S.; Burrows, P. E.; Thompson, M. E.; Forrest, S. R., Very high-efficiency green organic light-emitting devices based on electrophosphorescence. *Appl. Phys. Lett.* **1999,** *75* (1), 4-6.
30. Tsutsui, T.; Yang, M.-J.; Yahiro, M.; Nakamura, K.; Watanabe, T.; Tsuji, T.; Fukuda, Y.; Wakimoto, T.; Miyaguchi, S., High Quantum Efficiency in Organic Light-Emitting Devices with Iridium-Complex as a Triplet Emissive Center. *Jpn. J. Appl. Phys.* **1999,** *38* (Part 2, No. 12B), L1502-L1504.
31. Adachi, C.; Baldo, M. A.; Forrest, S. R.; Thompson, M. E., High-efficiency organic electrophosphorescent devices with tris(2-phenylpyridine)iridium doped into electron-transporting materials. *Appl. Phys. Lett.* **2000,** *77* (6), 904-906.
32. Lee, C.-L.; Lee, K. B.; Kim, J.-J., Polymer phosphorescent light-emitting devices doped with tris(2-phenylpyridine) iridium as a triplet emitter. *Appl. Phys. Lett.* **2000,** *77* (15), 2280-2282.
33. Holzer, W.; Penzkofer, A.; Tsuboi, T., Absorption and emission spectroscopic characterization of Ir(ppy)3. *Chem. Phys.* **2005,** *308* (1), 93-102.
34. Hofbeck, T.; Yersin, H., The Triplet State of *fac*-Ir(ppy)$_3$. *Inorg. Chem.* **2010,** *49* (20), 9290-9299.
35. Noda, H.; Nakanotani, H.; Adachi, C., Excited state engineering for efficient reverse intersystem crossing. *Sci. Adv.* **2018,** *4* (6), eaao6910.
36. Baryshnikov, G.; Minaev, B.; Ågren, H., Theory and Calculation of the Phosphorescence Phenomenon. *Chem. Rev.* **2017,** *117* (9), 6500-6537.
37. Shafikov, M. Z.; Kozhevnikov, D. N.; Bodensteiner, M.; Brandl, F.; Czerwieniec, R., Modulation of Intersystem Crossing Rate by Minor Ligand Modifications in Cyclometalated Platinum(II) Complexes. *Inorg. Chem.* **2016,** *55* (15), 7457-7466.
38. Kozhevnikov, D. N.; Kozhevnikov, V. N.; Shafikov, M. Z.; Prokhorov, A. M.; Bruce, D. W.; Williams, J. A., Phosphorescence vs fluorescence in cyclometalated platinum(II) and iridium(III) complexes of (oligo)thienylpyridines. *Inorg. Chem.* **2011,** *50* (8), 3804-3815.
39. Kozhevnikov, V. N.; Durrant, M. C.; Williams, J. A. G., Highly Luminescent Mixed-Metal Pt(II)/Ir(III) Complexes: Bis-Cyclometalation of 4,6-Diphenylpyrimidine As a Versatile Route to Rigid Multimetallic Assemblies. *Inorg. Chem.* **2011,** *50* (13), 6304-6313.
40. Yutaka, T.; Obara, S.; Ogawa, S.; Nozaki, K.; Ikeda, N.; Ohno, T.; Ishii, Y.; Sakai, K.; Haga, M.-a., Syntheses and Properties of Emissive Iridium(III) Complexes with Tridentate Benzimidazole Derivatives. *Inorg. Chem.* **2005,** *44* (13), 4737-4746.
41. Obara, S.; Itabashi, M.; Okuda, F.; Tamaki, S.; Tanabe, Y.; Ishii, Y.; Nozaki, K.; Haga, M.-A., Highly Phosphorescent Iridium Complexes Containing Both Tridentate Bis(benzimidazolyl)-benzene or -pyridine and Bidentate Phenylpyridine: Synthesis, Photophysical Properties, and Theoretical Study of Ir-Bis(benzimidazolyl)benzene Complex. *Inorg. Chem.* **2006,** *45* (22), 8907-8921.

42. Yang, W.-W.; Zhong, Y.-W.; Yoshikawa, S.; Shao, J.-Y.; Masaoka, S.; Sakai, K.; Yao, J.; Haga, M.-a., Tuning of Redox Potentials by Introducing a Cyclometalated Bond to Bis-tridentate Ruthenium(II) Complexes Bearing Bis(N-methylbenzimidazolyl)benzene or -pyridine Ligands. *Inorg. Chem.* **2012,** *51* (2), 890-899.
43. Herbst, A.; Bronner, C.; Dechambenoit, P.; Wenger, O. S., Gold Complexes with Tridentate Cyclometalating and NHC Ligands: A Search for New Photoluminescent Gold(III) Compounds. *Organomet.* **2013,** *32* (6), 1807-1814.
44. Shi, J.; Forsythe, E. W.; Morton, D. C. Method of making benzazoles. Patent US20130172570A1, 2012.
45. Dorazco-Gonzalez, A., Chemosensing of Chloride Based on a Luminescent Platinum(II) NCN Pincer Complex in Aqueous Media. *Organomet.* **2014,** *33* (4), 868-875.
46. Lanoe, P.-H.; Tong, C. M.; Harrington, R. W.; Probert, M. R.; Clegg, W.; Williams, J. A. G.; Kozhevnikov, V. N., Ditopic bis-terdentate cyclometallating ligands and their highly luminescent dinuclear iridium(III) complexes. *Chem. Commun.* **2014,** *50* (52), 6831-6834.
47. Shafikov, M. Z.; Daniels, R.; Pander, P.; Dias, F. B.; Williams, J. A. G.; Kozhevnikov, V. N., Dinuclear Design of a Pt(II) Complex Affording Highly Efficient Red Emission: Photophysical Properties and Application in Solution-Processible OLEDs. *ACS Appl. Mater. Interfaces* **2019,** *11* (8), 8182-8193.
48. Rausch, A. F.; Thompson, M. E.; Yersin, H., Matrix effects on the triplet state of the OLED emitter $Ir(4,6\text{-}dFppy)_2(pic)$ (FIrpic): investigations by high-resolution optical spectroscopy. *Inorg. Chem.* **2009,** *48* (5), 1928-1937.
49. Rausch, A. F.; Murphy, L.; Williams, J. A. G.; Yersin, H., Probing the Excited State Properties of the Highly Phosphorescent Pt(dpyb)Cl Compound by High-Resolution Optical Spectroscopy. *Inorg. Chem.* **2009,** *48* (23), 11407-11414.
50. Finkenzeller, W. J.; Thompson, M. E.; Yersin, H., Phosphorescence dynamics and spin-lattice relaxation of the OLED emitter $Ir(btp)_2(acac)$. *Chem. Phys. Lett.* **2007,** *444* (4-6), 273-279.
51. Czerwieniec, R.; Finkenzeller, W. J.; Hofbeck, T.; Starukhin, A.; Wedel, A.; Yersin, H., Photophysical properties of $Re(pbt)(CO)_4$ studied by high resolution spectroscopy. *Chem. Phys. Lett.* **2009,** *468* (4–6), 205-210.
52. Fischer, T.; Czerwieniec, R.; Hofbeck, T.; Osminina, M. M.; Yersin, H., Triplet state properties of a red light emitting [Pt(s-thpy)(acac)] compound. *Chem. Phys. Lett.* **2010,** *486* (1-3), 53-59.
53. Prokhorov, A. M.; Hofbeck, T.; Czerwieniec, R.; Suleymanova, A. F.; Kozhevnikov, D. N.; Yersin, H., Brightly luminescent Pt(II) pincer complexes with a sterically demanding carboranyl-phenylpyridine ligand: A new material class for diverse optoelectronic applications. *J. Am. Chem. Soc.* **2014,** *136* (27), 9637-9642.
54. Frisch, M. J.; Trucks, G. W.; Schlegel, H. B.; Scuseria, G. E.; Robb, M. A.; Cheeseman, J. R.; Scalmani, G.; Barone, V.; Mennucci, B.; Petersson, G. A.; Nakatsuji, H.; Caricato, M.; Li, X.; Hratchian, H. P.; Izmaylov, A. F.; Bloino, J.; Zheng, G.; Sonnenberg, J. L.; Hada, M.; Ehara, M.; Toyota, K.; Fukuda, R.; Hasegawa, J.; Ishida, M.; Nakajima, T.; Honda, Y.; Kitao, O.; Nakai, H.; Vreven, T.; Montgomery Jr., J. A.; Peralta, J. E.; Ogliaro, F.; Bearpark, M. J.; Heyd, J.; Brothers, E. N.; Kudin, K. N.; Staroverov, V. N.; Kobayashi, R.; Normand, J.; Raghavachari, K.; Rendell, A. P.; Burant, J. C.; Iyengar, S. S.; Tomasi, J.; Cossi, M.; Rega, N.; Millam, N. J.; Klene, M.; Knox, J. E.; Cross, J. B.; Bakken, V.; Adamo, C.; Jaramillo, J.; Gomperts, R.; Stratmann, R. E.; Yazyev, O.; Austin, A. J.; Cammi, R.; Pomelli, C.; Ochterski, J. W.; Martin, R. L.; Morokuma, K.; Zakrzewski, V. G.; Voth, G. A.; Salvador, P.; Dannenberg, J. J.; Dapprich, S.; Daniels, A. D.; Farkas, Ö.; Foresman, J. B.; Ortiz, J. V.; Cioslowski, J.; Fox, D. J., *Gaussian 09*. Gaussian, Inc.: Wallingford, CT, USA, 2009.

55. Peverati, R.; Truhlar, D. G., M11-L: A Local Density Functional That Provides Improved Accuracy for Electronic Structure Calculations in Chemistry and Physics. *J. Phys. Chem. Lett.* **2012,** *3* (1), 117-124.
56. Peverati, R.; Truhlar, D. G., Performance of the M11 and M11-L density functionals for calculations of electronic excitation energies by adiabatic time-dependent density functional theory. *Phys.Chem.Chem.Phys.* **2012,** *14* (32), 11363-11370.
57. Weigend, F.; Ahlrichs, R., Balanced basis sets of split valence, triple zeta valence and quadruple zeta valence quality for H to Rn: Design and assessment of accuracy. *Phys. Chem. Chem. Phys.* **2005,** *7* (18), 3297-3305.
58. Cossi, M.; Rega, N.; Scalmani, G.; Barone, V., Energies, structures, and electronic properties of molecules in solution with the C-PCM solvation model. *J. Comput. Chem.* **2003,** *24* (6), 669-681.
59. DFT optimization and TD-DFT calculations for complex 5 were also conducted with M06 functional. At this level the LUMO of complex 5 was predicted to be localized on the dpp ligand in both the ground state and the lowest triplet state optimized geometry. However, the absorption spectrum calcuated at this level of theory was not comparable to the experimental spectrum.
60. Turro, N. J.; Ramamurthy, V.; Scaiano, J. C., *Modern Molecular Photochemistry of Organic Molecules*. University Science Books: Saisalito, 2010; p 1084.
61. Montalti, M.; Credi, A.; Prodi, L.; Gandolfi, M. T., *Handbook of Photochemistry, Third Edition*. CRC Press: 2006; p 633.
62. Shi, S.; Jung, M. C.; Coburn, C.; Tadle, A.; Sylvinson M. R, D.; Djurovich, P. I.; Forrest, S. R.; Thompson, M. E., Highly Efficient Photo- and Electroluminescence from Two-Coordinate Cu(I) Complexes Featuring Nonconventional N-Heterocyclic Carbenes. *J. Am. Chem. Soc.* **2019,** *141* (8), 3576-3588.
63. Shafikov, M. Z.; Suleymanova, A. F.; Czerwieniec, R.; Yersin, H., Design Strategy for Ag(I)-Based Thermally Activated Delayed Fluorescence Reaching an Efficiency Breakthrough. *Chem. Mater.* **2017,** *29* (4), 1708-1715.
64. Shafikov, M. Z.; Suleymanova, A. F.; Czerwieniec, R.; Yersin, H., Thermally Activated Delayed Fluorescence from Ag(I) Complexes: A Route to 100% Quantum Yield at Unprecedentedly Short Decay Time. *Inorg. Chem.* **2017,** *56* (21), 13274-13285.
65. Shafikov, M. Z.; Suleymanova, A. F.; Schinabeck, A.; Yersin, H., A di-nuclear Ag(I) complex designed for highly efficient thermally activated delayed fluorescence. *J. Phys. Chem. Lett.* **2018,** *9*, 702-709.
66. Wallesch, M.; Volz, D.; Zink, D. M.; Schepers, U.; Nieger, M.; Baumann, T.; Bräse, S., Bright Coppertunities: Multinuclear Cu^{I} Complexes with N–P Ligands and Their Applications. *Chem. Eur. J.* **2014,** *20* (22), 6578-6590.
67. Leitl, M. J.; Krylova, V. A.; Djurovich, P. I.; Thompson, M. E.; Yersin, H., Phosphorescence versus Thermally Activated Delayed Fluorescence. Controlling Singlet-Triplet Splitting in Brightly Emitting and Sublimable Cu(I) Compounds. *J. Am. Chem. Soc.* **2014,** *136* (45), 16032-16038.
68. Hofbeck, T.; Monkowius, U.; Yersin, H., Highly Efficient Luminescence of Cu(I) Compounds: Thermally Activated Delayed Fluorescence Combined with Short-Lived Phosphorescence. *J. Am. Chem. Soc.* **2015,** *137* (1), 399-404.
69. Hamze, R.; Peltier, J. L.; Sylvinson, D.; Jung, M.; Cardenas, J.; Haiges, R.; Soleilhavoup, M.; Jazzar, R.; Djurovich, P. I.; Bertrand, G.; Thompson, M. E., Eliminating nonradiative decay in Cu(I) emitters: >99% quantum efficiency and microsecond lifetime. *Science* **2019,** *363* (6427), 601.
70. Volz, D.; Chen, Y.; Wallesch, M.; Liu, R.; Fléchon, C.; Zink, D. M.; Friedrichs, J.; Flügge, H.; Steininger, R.; Göttlicher, J.; Heske, C.; Weinhardt, L.; Bräse, S.; So, F.; Baumann, T., Bridging the Efficiency Gap: Fully Bridged Dinuclear Cu(I)-Complexes for Singlet Harvesting in High-Efficiency OLEDs. *Adv. Mater.* **2015,** *27* (15), 2538-2543.

71. Zeng, W.; Zhou, T.; Ning, W.; Zhong, C.; He, J.; Gong, S.; Xie, G.; Yang, C., Realizing 22.5% External Quantum Efficiency for Solution-Processed Thermally Activated Delayed-Fluorescence OLEDs with Red Emission at 622 nm via a Synergistic Strategy of Molecular Engineering and Host Selection. *Adv. Mater.* **2019**, e1901404.
72. Hamze, R.; Shi, S.; Kapper, S. C.; Muthiah Ravinson, D. S.; Estergreen, L.; Jung, M.-C.; Tadle, A. C.; Haiges, R.; Djurovich, P. I.; Peltier, J. L.; Jazzar, R.; Bertrand, G.; Bradforth, S. E.; Thompson, M. E., "Quick-Silver" from a Systematic Study of Highly Luminescent, Two-Coordinate, d^{10} Coinage Metal Complexes. *J. Am. Chem. Soc.* **2019,** *141* (21), 8616-8626.

TOC Graphics